Computers & Fluids 100 (2014) 218–226

Contents lists available at ScienceDirect

Computers & Fluids

journal homepage: www.elsevier.com/locate/compfluid

Droplet formation via squeezing mechanism in a microfluidic flow-focusing device

Amit Gupta [a,*], Harpreet S. Matharoo [a], Devavret Makkar [a], Ranganathan Kumar [b]

[a] Department of Mechanical Engineering, Indian Institute of Technology Delhi, Hauz Khas, New Delhi 110016, India
[b] Department of Mechanical, Materials and Aerospace Engineering, University of Central Florida, Orlando, FL 32816, USA

ARTICLE INFO

Article history:
Received 29 June 2013
Received in revised form 26 April 2014
Accepted 17 May 2014
Available online 27 May 2014

Keywords:
Lattice Boltzmann
Microfluidics
Flow-focusing
Droplet formation

ABSTRACT

In this work, the formation of droplets in a microfluidic flow-focusing device is studied and presented. Spurious velocities at the fluid–fluid interface were found to be very small in the lattice Boltzmann simulations. Using this technique, simulations have been performed to study the effect of geometry on formation of droplets for a microfluidic flow-focusing device. The effect of orifice width, orifice length and distance of the orifice on the mechanism of droplet formation and size of droplets is presented for different Capillary numbers. It is shown that, for $Ca \ll 1$, creation of droplets proceeds through the squeezing process that has earlier been observed in the T-junction configuration. The size of droplets increases with an increase in the (a) width, and (b) distance of orifice from the inlet. On increasing orifice length, droplet size first decreases to a minimum and increases thereafter. This study also reveals that the size of droplets becomes independent and approaches a constant beyond a critical value of the orifice length.

© 2014 Elsevier Ltd. All rights reserved.

1. Introduction

Different methods of forming microsized droplets using passive breakup has been a focus of active research for the past two decades. Microscale droplets formed in a controlled size and frequency are particularly useful in a wide range of applications, such as food processing, drug delivery, tumor destruction, performing chemical reactions, in creation of emulsions, personal health care products and bubble generators [1,2]. There are a variety of devices that can be used to generate droplets at the microscopic scale. Primarily, three device geometries have received significant attention: using coflowing fluids [3,4], droplet formation at T-junction [5–9,10], and passing immiscible fluids through an orifice [11,12,13,14,15,16].

A microfluidic flow-focusing device combines the flow-focusing geometry into a microchannel, a schematic of which is shown in Fig. 1. As is shown, there exist three flow inlets to the device: the outer ones carry the continuous fluid and the inner one carries the to-be-dispersed fluid. As the two immiscible liquids interact, the three streams are made to pass through a narrow orifice placed at a distance from the inlet. Depending upon the flow and geometrical parameters, the interaction of the fluids results in the breakup of the inner liquid stream into droplets, which then flow downstream into the collection tube.

In one of the earliest studies conducted on the flow-focusing device, droplet formation scenarios for different flow regimes was documented by Anna et al. [11]. These experiments were conducted on a fixed geometry for different flow rate ratios using a combination of silicone oil (with surfactants to discourage coalescence of droplets formed past a narrow orifice) and water. Different regimes were observed, with droplet sizes ranging from the width of orifice to much smaller droplets of monodisperse to polydisperse distributions. Garstecki et al. [13], through experiments on the microfluidic flow-focusing device, provided evidence that the dynamics of the interface are dictated by inertia of the flow. More recently, Romero and Abate [15] have shown that droplet formation for low to moderate Capillary numbers in the flow-focusing device occurs as a result of plugging-squeezing process, similar to that observed in a T-junction device.

Numerical study of the flow-focusing device has also received some attention. Jensen et al. [14], using a Stokes' flow representation of the liquid phase, presented the dynamics of formation of gas bubbles in an axisymmetric flow-focusing device. Their results were used to derive a scaling law for the volume of bubbles created. Zhou et al. [16] studied the flow-focusing device through an adaptive meshing phase-field model. The mechanism of droplet formation for some of the observed flow regimes was explained. Scaling laws for dependence of droplet radius on the Bond number

* Corresponding author. Tel.: +91 11 2659 1270; fax: +91 11 26582053.
E-mail address: agupta@mech.iitd.ac.in (A. Gupta).

http://dx.doi.org/10.1016/j.compfluid.2014.05.023
0045-7930/© 2014 Elsevier Ltd. All rights reserved.

Nomenclature

c_s	speed of sound
C	color distribution variable
Ca	$\mu_c U_0/\sigma$, Capillary number
d^*	d/h_i, non-dimensionalised orifice width
d	width of orifice
$\vec{e}_i$	phase space velocity vector
f^a	particle distribution of fluid a
f^t	particle distribution after collision
$\vec{F}$	interfacial force
h_f^*	h_f/h_i, non-dimensionalised orifice distance from inlet
h_c	channel width of collecting tube
h_i	channel width of to-be-dispersed phase
h_0	channel width of continuous phase
l_{or}^*	l_{or}/h_i, non-dimensionalised orifice length
l_{or}	length of orifice
$\vec{n}$	normal to surface
n_x	number of lattice units along x-axis
n_y	number of lattice units along y-axis
Q_d	flow rate of dispersed phase
Q_c	flow rate of continuous phase
Q	Q_d/Q_c, flow rate ratio
U_0	average velocity of continuous phase

Greek symbols

β	anti-diffusion parameter
ρ	density of the fluid
ρ_r	density of the red fluid
ρ_b	density of the blue fluid
κ	local curvature
τ	relaxation time
∇_s	surface gradient operator
Φ_i	source term
σ	surface tension
μ_d	viscosity of dispersed phase
μ_c	viscosity of continuous phase
Λ	μ_d/μ_c, viscosity ratio

and flow rate ratio were given, which were shown to agree with their simulation results. It was also shown that inclusion of two extra channels to the geometry could be used to form compound droplets. Dupin et al. [12] have developed a lattice Boltzmann based framework that controls the coalescence of droplets formed downstream of the orifice in a flow-focusing device.

However, despite these studies, the effect of geometry of a flow-focusing device on droplet formation behavior has not received any attention. The dimensions and orifice position in the device can play an important role in destabilizing the interface and enforcing breakup. An understanding of the geometry and its influence on size of droplets formed can assist in meeting required targets for microfluidics devices. Thus, the objectives of this study are:

(1) Identify the mechanism through which formation of droplets occurs in a flow-focusing device at low Capillary numbers, and
(2) Quantify the dependence of droplet size on the size and location of the orifice in a flow-focusing device.

As shown in Fig. 1, three different geometrical parameters are associated with a flow-focusing device. These are the width of the orifice (d), the length of the orifice (l_{or}) and the distance of the orifice from inlet channels (h_f). Simulations for different Capillary numbers for a wide range of each of the three geometric parameters are conducted and presented.

2. Methodology

The simulation of multiphase flows can be performed using the front-capturing/diffuse-interface (for e.g., marker-and-cell, volume-of-fluid, level-set, lattice Boltzmann) or the front-tracking (for e.g., boundary integral) methods. The diffuse-interface methods are easy to model and can accommodate large surface topology changes, whereas the front-tracking methods tend to suffer from singularities that occur due to a rapidly evolving interface. In the present study, our focus has been on implementing a lattice Boltzmann based multicomponent model to simulate the droplet formation process in a two-dimensional microfluidic flow-focusing device.

2.1. Lattice Boltzmann method (LBM)

In recent years, the lattice Boltzmann method has emerged as a promising numerical technique to model fluid flows. LBM has been proven to be particularly successful in modeling fluid flows involving complex boundaries and interfacial dynamics. This method is based on microscopic kinetic equations that solve for the distribution function(f) of the fluid. The governing equations are such that the essential physics of mesoscopic processes is incorporated, and at the same time the averaged properties obey the macroscopic governing equations. The simplified kinetic model can accurately predict the flow behavior since the macroscopic fluid dynamics is the result of microscopic behavior of the particles of system collectively [17].

LBM modeling of fluid flows has several benefits over the conventional Navier–Stokes based simulation methods. For example, in LBM a linear partial differential equation is solved which is relatively easier than the Navier–Stokes equation in which convective terms lead to a non-linear partial differential equation. Also, static pressure in LBM is solved by using the equation of state, while in Navier–Stokes modeling it is calculated by solving the Poisson's

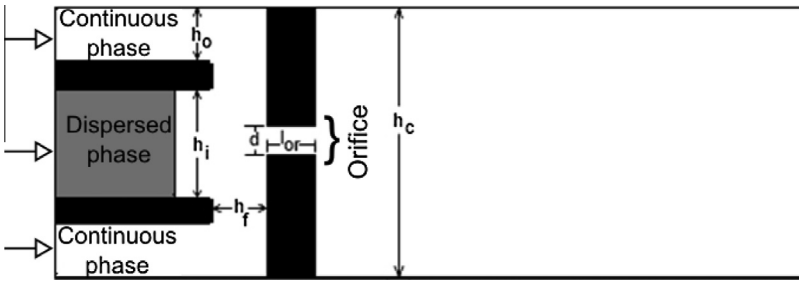

Fig. 1. Schematic diagram of flow focusing device.

equation which requires special treatments such as iteration or relaxation. Last but not the least, no matrix inversions are required in LBM due to the local nature of the governing equation, thereby making it ideal for parallelization [17].

In this study, a diffuse interface lattice Boltzmann method for biphasic flow has been employed to model the flow in the microfluidic device [18]. The method has the ability to accommodate surface topology changes including interface break-up and coalescence. Another attractive feature of the model is the small magnitude of spurious currents that occur at the interface of the two fluids [7].

In LBM, the evolution of the flow is simulated by performing two operations at each time step: collision and streaming. At the end of the collision step, the particle distribution of the fluid in consideration acquires directions of translation or streaming. The value of a temporary distribution variable f_i^t is given by Eq. (1).

$$f_i^t(\vec{x}, t+\delta_t) = f_i(\vec{x}, t) + \frac{1}{\tau_f}(f_i^{eq} - f_i) \tag{1}$$

In the streaming step, the variables surrounding the current lattice are assigned the particle distributions which were calculated in the collision step, as shown in Eq. (2).

$$f_i(\vec{x} + \vec{e_i}\,\delta_t, t+\delta_t) = f_i^t(\vec{x}, t+\delta_t) \tag{2}$$

When this method is applied on multiphase flows, the distribution variables are defined for all the phases separately. In the current case, there are two immiscible phases or fluids which are denoted by the 'red' and 'blue' color. Then color distribution variable 'C' is defined based on the density of the two fluids in Eq. (3),

$$C = \frac{\rho_r - \rho_b}{\rho_r + \rho_b} \tag{3}$$

Here, ρ_r and ρ_b are the densities of the red and blue fluid, respectively. Clearly, the value of color function remains constant in the pure fluid regions and changes across the interface, where the two fluids coexist. Moreover, the macroscopic properties of the fluid can be recovered through zeroth- and first-order closure of the distribution function,

$$\sum_i f_i = \rho \tag{4}$$

$$\sum_i f_i \vec{e}_i = \rho \vec{U} \tag{5}$$

The local curvature on the interface is computed based on the components of the local normal vector. The normal vector $\vec{n}$ is computed based on the color gradient using Eq. (6).

$$\vec{n} = -\frac{\nabla C}{|\nabla C|} \tag{6}$$

Based on the local normal vector, the curvature (κ) at any location is computed using Eq. (7).

$$\kappa = \frac{1}{R} = -\nabla_s \cdot \vec{n} \tag{7}$$

Here, ∇_s is the surface gradient operator which calculates the gradient tangent to the surface. Based on the curvature, the source term Φ_i is calculated such that it incorporates the surface tension force, given by Eq. (8).

$$\Phi_i = \frac{\gamma_i}{c_s^2}\vec{F} \cdot \vec{e_i} \tag{8}$$

where γ_i are the weights assigned to the equilibrium distribution function [8]. Here, the interfacial force $\vec{F}$ is given by Eq. (9).

$$\vec{F}(\vec{x}, t) = -\frac{1}{2R}\sigma \nabla C \tag{9}$$

The partial derivatives of any function g are calculated by discretizing it on a regular lattice using values from neighboring lattice nodes. The expression for partial derivative in a direction x_j is given in Eq. (10).

$$\frac{\partial g}{\partial x_j} = \frac{1}{c_s^2}\sum_i g(x + e_i) e_{ix_j} \gamma_i \tag{10}$$

Color separation is applied to the post-collision distribution to sharpen the interface, further reduce the spurious velocities and eliminate lattice pinning [19,18]. The distributions of the two color fluids are calculated by Eq. (11).

$$\begin{pmatrix} f_i^r \\ f_i^b \end{pmatrix} = \frac{1}{(\rho_r + \rho_b)} f_i \begin{pmatrix} \rho_r \\ \rho_b \end{pmatrix} \pm \gamma_i \beta \frac{\rho_r \rho_b}{(\rho_r + \rho_b)} \vec{e_i} \cdot \vec{n} \tag{11}$$

where β is the antidiffusion parameter, taken to be 0.7 to keep spurious velocities low and maintain a sharp interface [7,19].

3. Results and discussion

Before conducting simulations on the microfluidic flow-focusing device, a preliminary analysis of the multiphase model was performed by conducting static bubble tests. Two-dimensional simulations were run with the initial condition as uniform pressure throughout the domain and periodic boundary conditions an all boundaries for different initial diameters. The domain was discretized into 250×250 lattice points. Simulations were run till equilibrium was reached and a pressure gradient was generated across the interface. To validate the multiphase model, the predictions of the simulations were compared with Laplace's law, which states that the pressure difference across the interface of a static bubble is proportional to the curvature of the interface and surface tension. The general formula for a droplet in three-dimensions is $P_{in} - P_{out} = \sigma\left(\frac{1}{r_1} + \frac{1}{r_2}\right)$, which reduces to $P_{in} - P_{out} = \frac{2\sigma}{r}$ for a spherical droplet [20]. In two-dimensions, one of the radii of curvature goes to infinity, i.e. r2 $\rightarrow \infty$, which would lead to

$$P_{in} - P_{out} = \frac{\sigma}{r} \tag{14}$$

Here, r is the mean radius and σ is the surface tension. A linear dependence (not shown here) between pressure differential across the interface vs. curvature was recorded for low values of curvature, which indicated that the current model correctly incorporates the stress boundary condition at the two-fluid interface. However, the linear dependence deviated from the Laplace's law at higher values of curvatures when the interface width becomes comparable to the radius (i.e. $r \approx 3\Delta x$), thus reducing the accuracy of the model. Consequently, the lattice resolution selected for flow-focusing simulations was such that the minimum diameter of droplets formed is never allowed to drop below 5 grid units.

Subsequently, the numerical method was validated against the published results of Shi et al. [21] who modeled the flow in a microfluidic flow-focusing device using a lattice Boltzmann framework. Simulations were conducted for $Ca = 0.036$ for the geometry modeled in their work. As shown in Fig. 2, a comparison of droplet sizes obtained from the simulations of the present study with Shi et al. [21] shows good agreement. For LBM simulations, no-slip boundary conditions were employed using the second-order accurate half-way bounceback scheme for the solid walls. The dispersed phase is non-wetting and the continuous phase wets the solid wall in the main channel. At the inlet and outlet, mass flux was prescribed at each time increment using $f_i^{eq}(\rho, \mathbf{u}_{inlet})$. In addition, a constant outlet pressure was enforced at the exit and the pressure at the inlet was allowed to develop to a steady-state value [22]. For each simulation, the CPU time to complete a single run on an Intel Xeon chip of speed 2.40 GHz was approximately 6 h.

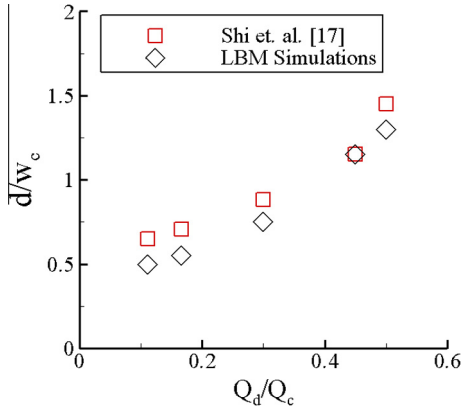

Fig. 2. Comparison of droplet size from the current simulations with Shi et al. [19] for $Ca = 0.036$ and $\lambda = 1/4$.

In addition to validation against [21], the simulation results are also found to be in qualitative agreement with Anna et al. [11] who also reported large spherical droplets which were nearly the size of the continuous phase channel width (i.e., h_o) formed for low continuous phase flow rates. However, a direct comparison was not possible as they used silicone oil with surfactants (to limit the coalescence of water droplets formed downstream of the channel) for which the exact interfacial tension was not reported.

A grid independence test was conducted to establish the minimum number of lattices which would be required to accurately resolve the interface and predict the size and shape of the droplets formed. Simulations were run for different number of lattices, while the geometry and flow conditions were kept fixed. Droplet size for each simulation was calculated and tabulated against the corresponding mesh size as shown in Table 1. For these simulations, the parameters were chosen as $Ca = 0.01$, $Q = 1/4$, and $\Lambda = 1/6$. Here n_x and n_y are the number of lattices in x and y directions respectively. The refinement of the domain from 39,200 lattices to 129,600 lattices (decrease of lattice spacing by ~230%) led to a change in droplet volume (per unit depth) of 2.6%. Since the change was within 5%, the use of a coarser mesh to save time was found to be justified.

A representative case of LBM simulation for droplet formation in a microfluidic flow-focusing device is shown in Fig. 3. The simulation was run for $Ca = 0.01, Q = 1/4, \Lambda = 1/6, l^*_{or} = 0.25, h^*_f = 0.5$ and $d^* = 0.375$. As shown in Fig. 3, the dispersed liquid stream first forms a bulb as it enters the device, which continues to grow until it reaches the orifice. The blockage created by the plug causes the pressure upstream of the orifice to rise, which leads to "squeezing" of the interface (as shown in Fig. 3(c)) and the dispersed fluid is focused into a thin thread. The fluid collected in the bulb and the fluid from the source continue to pass through this stream and form a bulb downstream of the orifice. At the same time, the connecting liquid thread continues to thin. After a short time duration, the thread ruptures and gives birth to a droplet, which is then carried downstream in the collection tube.

Table 1
Non-dimensional droplet volume (per unit depth) vs. total number of lattices.

$n_x n_y$	Non-dimensional droplet volume per unit depth
39,200	0.33
78,400	0.328
129,600	0.339

3.1. Parametric study

For the purpose of outlining the role of geometry of the device, a detailed study on its effect on droplet formation has been conducted. The same geometry as one taken for grid independence test is used. The effect of each geometric parameter on droplet formation has been studied for a range of Capillary numbers by varying the parameter of interest, while others are kept fixed. The parameters which have been varied are non-dimensional orifice width (d^*) orifice length (l^*_{or}) and distance of orifice from inlet (h^*_f). The following flow parameters are held fixed in this study: flow rate ratio $Q_d/Q_c = 1/4$ and viscosity ratio $\mu_d/\mu_c = 1/6$. Ca has been chosen to be much less than 1 so as to be confined to the squeezing regime of droplet formation [1,7]. The flow rate ratio has been selected based on reported values for which monodisperse droplet formation was reported in the literature [11]. The viscosity ratio has been selected to match that of water and silicone oil system where the viscosity ratio is nearly 1/6. The continuous phase Reynolds number is kept $\leqslant 1$. The effect of variation in the Capillary number has been studied by performing simulations at three different conditions of $Ca = 0.01$, $Ca = 0.0075$ and $Ca = 0.005$.

3.1.1. Effect of orifice length (l^*_{or})

Simulations have been conducted for a range of orifice lengths to quantify its effect on the size of droplets formed. Fig. 4 shows a plot of non-dimensionalized droplet volume (per unit depth) vs. orifice length for different Capillary numbers. The droplet volume (per unit depth) has been normalized using h_i^2. Based on these results, it can be observed that as the Capillary number increases, droplets of a smaller size are formed. For each Capillary number a minimum and a maximum droplet sizes occur at finite values of the orifice length, with the critical orifice length for the minimum sized droplet decreasing in magnitude. As the orifice length is shortened, the size of droplets tends to grow exponentially; for a long orifice, it approaches a constant value. However, the range of Ca considered in the present study is not wide enough to be able to discern a universal trend due to which it is not known if a maximum in droplet size would ever be reached if the Ca is reduced even further.

Figs. 5 and 6 show different stages in the formation of droplets for two disparate lengths of the orifice. For the case of the longer length orifice (i.e., $l^*_{or} = 1.5$), the droplet travels in the orifice after pinch-off, as shown in Fig. 6(c).

The sudden growth in droplet size for decreasing orifice lengths, as shown in Fig. 4, needs further discussion. A comparison of the continuous phase pressure recorded upstream of the orifice for $Ca = 0.01$ for two different orifice lengths corresponding to $l^*_{or} = 0.0625$ and $l^*_{or} = 1.5$ is shown in Fig. 7. For $l^*_{or} = 0.0625$ and with reference to Fig. 7(a), the pressure build-up in the continuous phase is gradual and reaches a maximum when the dispersed phase passes through, emerges on the downstream side and has completely blocked the orifice (as shown in the inset images (A) and (B)). At this instant of time, the lack of a solid obstruction (wall) downstream of the orifice presents the dispersed phase with an opportunity to expand forming a bulb while the upstream neck is gradually squeezed due to the high pressure in the continuous phase (inset image (C)). As the neck is squeezed, a portion of the orifice passage (that was earlier occupied by the dispersed phase) is opened for the flow of the continuous phase due to which the pressure decreases gradually. This process culminates with the neck and the bulb separating out resulting in the formation of a large spherical droplet (inset images (D) and (E)), the opening of the orifice for the passage of continuous phase and the reduction in its pressure. Unlike for short orifice lengths and as shown in inset images of Fig. 7(b), the dispersed phase penetrates the orifice section and is confined by the solid walls, thereby not allowing the

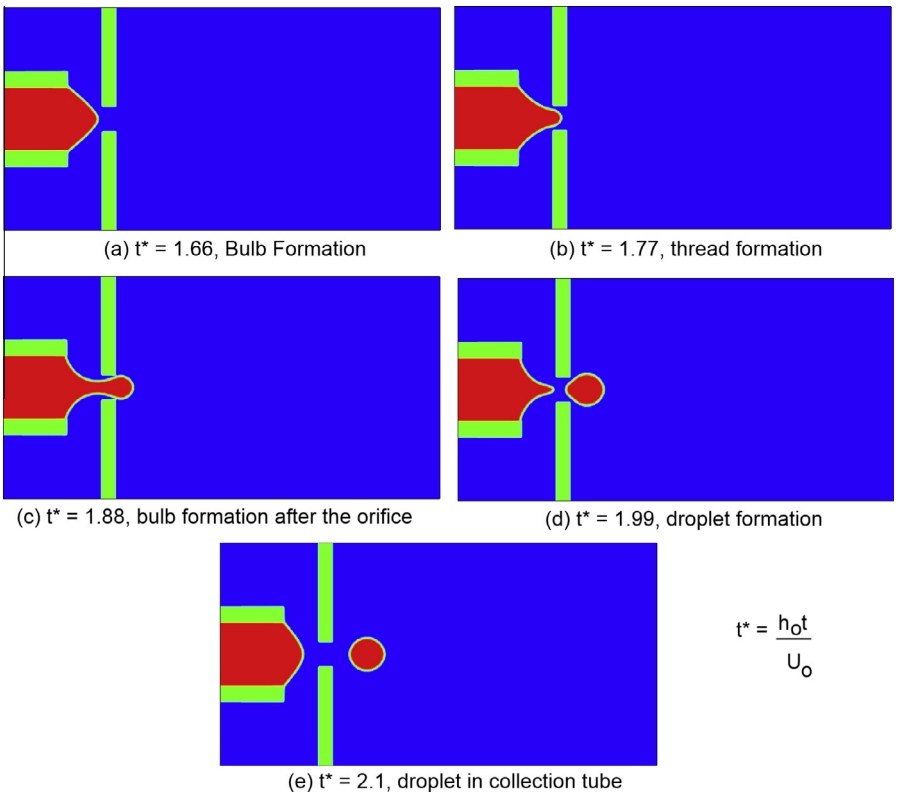

Fig. 3. Mechanism of droplet formation in a flow focusing device for $Ca = 0.01$, $l^*_{or} = 0.25$, $h^*_f = 0.5$ and $d^* = 0.375$.

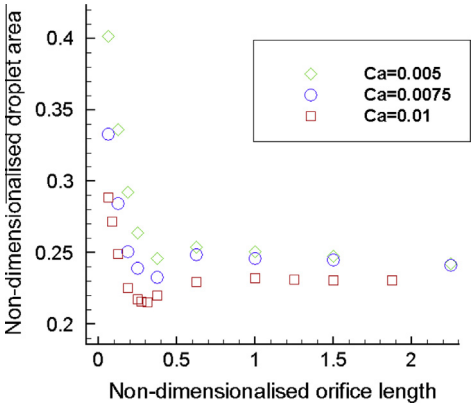

Fig. 4. Droplet area vs. length of orifice for different Capillary numbers.

formation of a bulb in an orifice with a longer length (inset images (A) and (B)). After some time, the thread connecting the bulb of the dispersed phase with the incoming liquid becomes very thin, leading to pinch-off even before droplet has travelled to the end of the orifice and started to expand (inset image (C)). Hence, the pressure decreases rapidly due to the continuous phase rushing into the orifice opening, indicating that the squeezing of the dispersed phase at the orifice entrance precedes a steep drop in pressure. Subsequently, the pressure increases due to the blockage of the flow of continuous fluid through the orifice which remains occupied by the dispersed phase plug (inset image (D)). These results indicate that orifice lengths longer than a critical length do not have any effect on the throughput from the device.

To explain the presence of a minimum in droplet size, the earlier arguments can be extended. Starting from a short orifice, as the length of the orifice is increased, the droplet size decreases. At a certain length of the orifice, the dispersed stream is stretched to a critical length in the orifice, where the dispersed phase in the orifice housing is just short of reaching the collecting tube on the other end, thereby losing the opportunity to expand. At this critical length, the size of the droplet formed is a minimum. Additionally, it is clear that with a decrease in *Ca*, the droplet size is bound to increase as the interfacial tension dominates over the continuous phase pressure build-up ($\because Ca \propto \sigma^{-1}$). Therefore, the interface travels a longer distance inside the orifice before a drop is formed with decrease in Ca. Hence, the minimum droplet area location shifts to the right with decreasing Capillary number.

3.1.2. Effect of orifice width (d^*)

The effect of orifice width on the mechanism of droplet formation is also investigated. Fig. 8 shows the dependence of droplet volume (per unit depth) on orifice width for different Ca. As can be observed, the size of droplets formed increases non-linearly with increasing orifice width. Also, for the same orifice width, droplets of smaller size were formed as *Ca* increases, with the relative increase largest for orifices with a large width.

The mechanism of droplet formation in a flow-focusing device involves focusing of the dispersed liquid stream into a thread, which eventually breaks up into small droplets because of hydrodynamics forces. The droplet formation process for two very different orifice widths of $d^* = 0.175$ and 0.75 from the perspective of increase in upstream continuous phase pressure has been studied and is shown in Fig. 9. The inset images show the stages during the droplet formation as the dispersed phase penetrates the orifice. For $d^* = 0.175$, three distinct peaks in the continuous phase pressure are observable. The first pressure peak (shown as inset (A)) corresponds to the dispersed phase blocking the orifice. After a short duration, a primary droplet is formed. The second peak (inset (B)) appears as the interface does not recede out of the orifice and hence a smaller satellite droplet is also formed. Subsequently, a

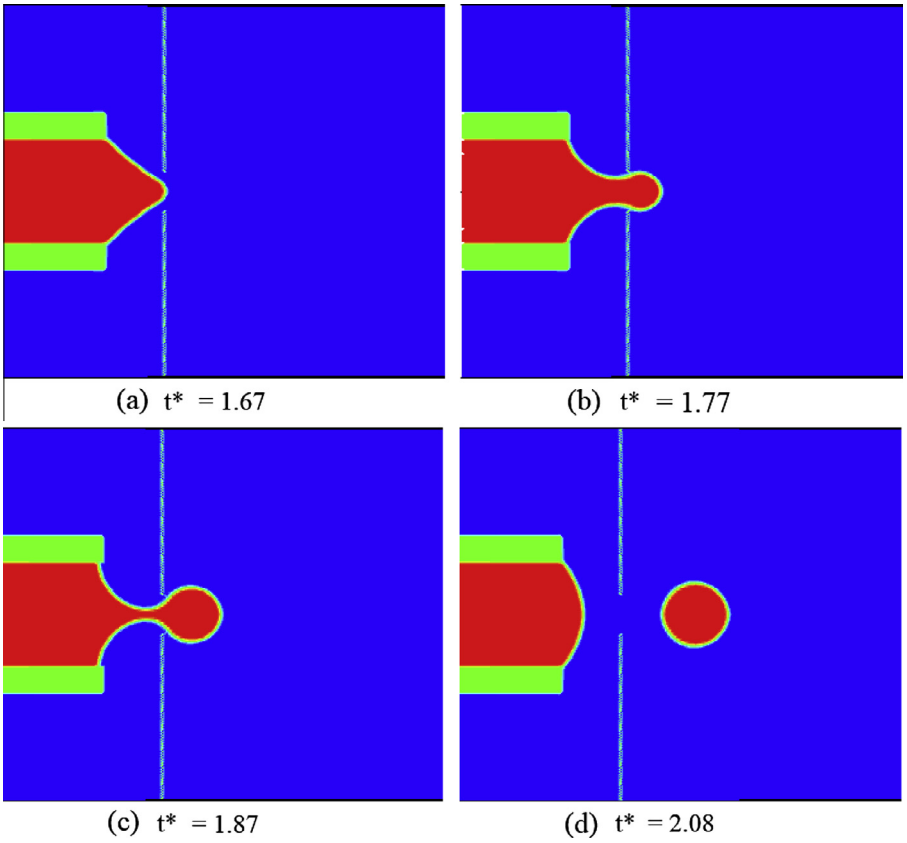

Fig. 5. Droplet formation in flow focusing device for $Ca = 0.01$, $l^*_{or} = 0.0625, h^*_f = 0.5$, $d^* = 0.375$.

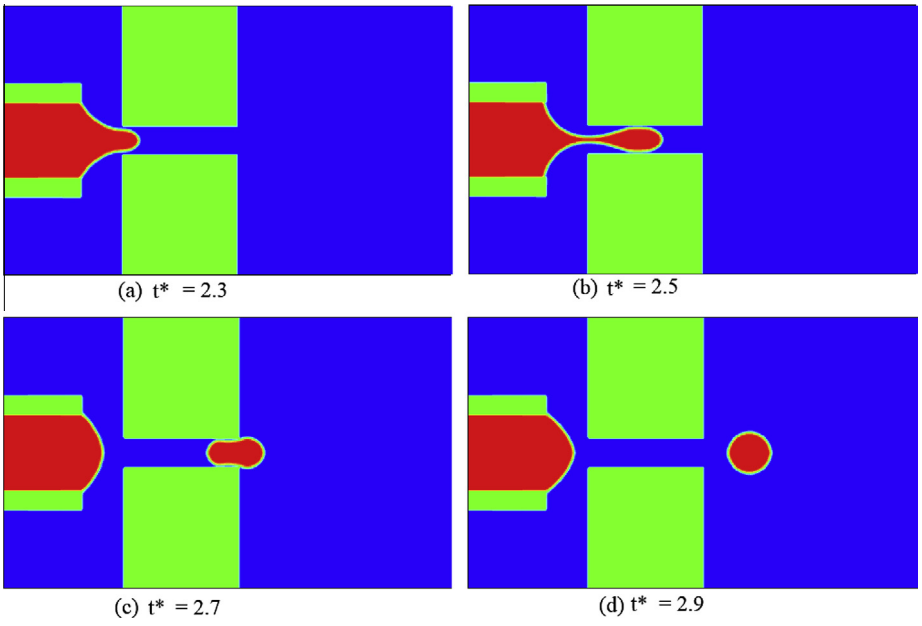

Fig. 6. Droplet formation in flow focusing device for $Ca = 0.01$, $l^*_{or} = 1.5, h^*_f = 0.5$, $d^* = 0.375$.

third peak appears in which a second satellite droplet is formed as well. The three droplets combine to form one larger droplet (inset (C)) that travels downstream and the interface retreats (inset (D)). However, for $d^* = 0.75$, the droplet formation process is spread over a longer time duration in which the interface emerges on the downstream side of the orifice (inset (I)), the pressure squeezes the interface to reduce the neck thickness (inset (J)), and finally a large spherical droplet is formed downstream and the pressure drops (inset (K)).

The remarkable difference in sizes of droplet formed clearly suggests that for an orifice with a wider opening (i.e. large d^*), confinement of the dispersed fluid is reduced considerably. Thereby,

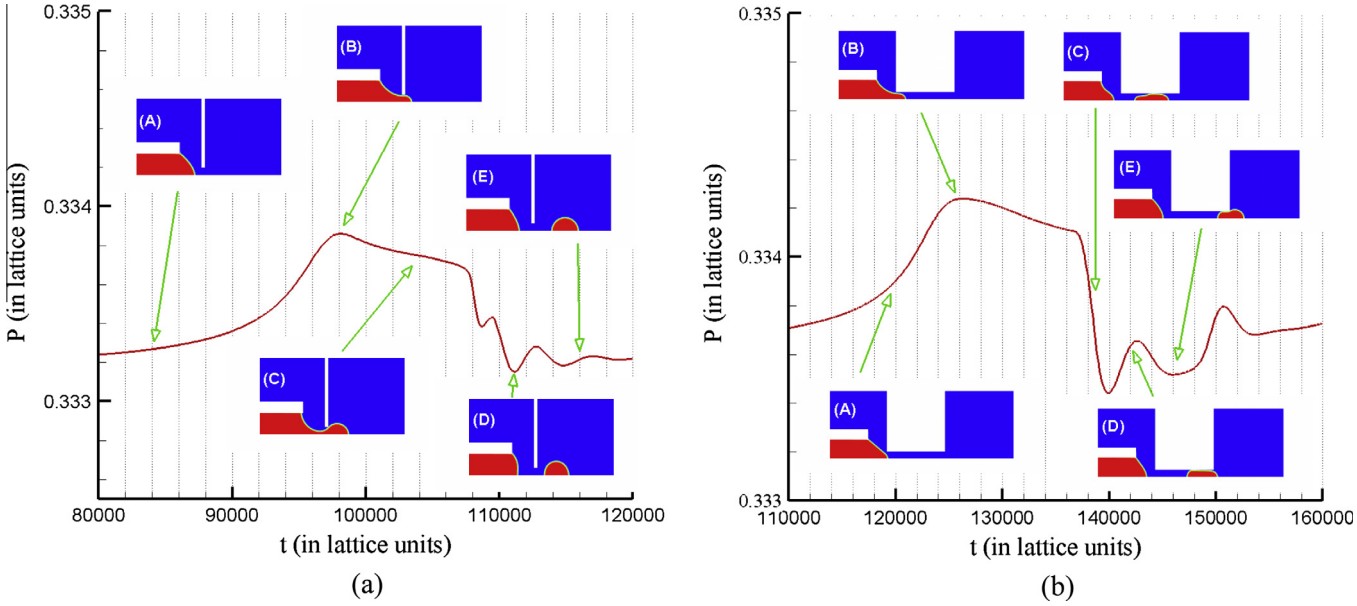

Fig. 7. Pressure variation for two different droplet formation scenarios corresponding to (a) $l^*_{or} = 0.0625$ and (b) $l^*_{or} = 1.5$ for $Ca = 0.01$, $d^* = 0.375$ and $h^*_f = 0.5$. Inset images show the contours of density of dispersed (red) and continuous phases (blue) at selected time instants shown by the arrows. Only the upper half domain is shown for better utilization of space. (For interpretation of the references to color in this figure legend, the reader is referred to the web version of this article.)

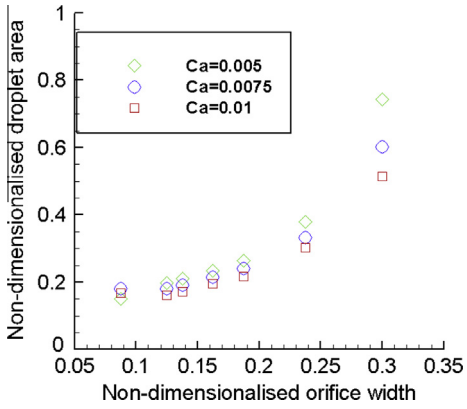

Fig. 8. Droplet area vs. orifice width for different Capillary numbers.

the pressure in the continuous phase stream is not allowed to build up sufficiently where squeezing of the plug can take place. Although not shown here, and similar to a T-junction configuration [9], for even higher flow rates of the dispersed phase, a transition to parallel flow occurs because of the combined effect of low pressure build-up upstream of the orifice and thicker threads emerging out of the orifice.

3.1.3. Effect of distance of orifice from Inlet (h^*_f)

The last parameter considered for the parametric analysis is the distance of the orifice from the inlet (shown as h_f in Fig. 1). Fig. 10 shows the dependence of droplet area on h^*_f for different Ca. As shown in the figure, and similar to the dependence on d^*, the droplet size increases as the distance of the orifice from continuous phase channel is increased. Also, for the same geometry (i.e., same h^*_f), droplets of smaller size are observed as the Capillary number is increased. However, the effect of Ca on droplet size is only pronounced when the orifice is placed at a distance more than the dispersed phase channel width (i.e., $h^*_f \geq 1$). Thus, increasing the separation between the inlet channels and the orifice opening can be an effective way of producing larger droplets even at $Ca \sim 0.01$.

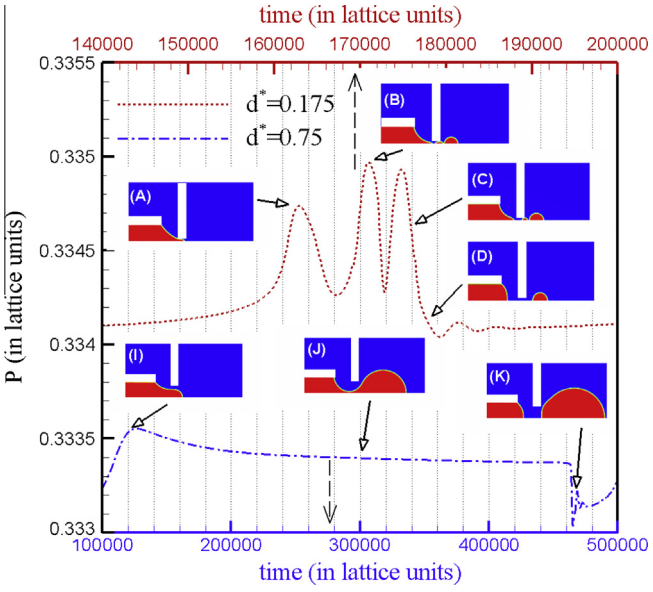

Fig. 9. Pressure variation for two different geometries corresponding to $d^* = 0.175$ and $d^* = 0.75$ for $Ca = 0.01$. Inset images show the contours of density at selected time instants shown by the arrows for the upper half domain only. The abscissa for the former is on top (in red) and for the latter is at the bottom (in blue) and are indicated by dotted arrows. (For interpretation of the references to color in this figure legend, the reader is referred to the web version of this article.)

To study the increase in droplet size with increasing distance from continuous phase channel, a comparison of continuous phase pressure upstream of the orifice is shown for two different h^*_f in Fig. 11. As earlier, also shown in insets are snapshots of the droplet formation process at different time instants. For $h^*_f = 0.375$, the dispersed phase has to travel a shorter distance to reach the orifice entrance. When the dispersed phase enters and blocks the orifice (inset (A)), the continuous phase pressure begins to rise rapidly. Thereafter, the squeezing of the dispersed phase by the continuous liquid begins due to which the interface is displaced towards the center of the orifice and the pressure begins to decrease. At a later

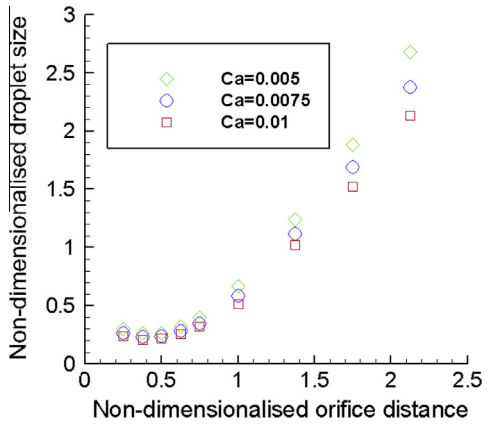

Fig. 10. Droplet area vs. distance of orifice from the inlet for different Capillary numbers.

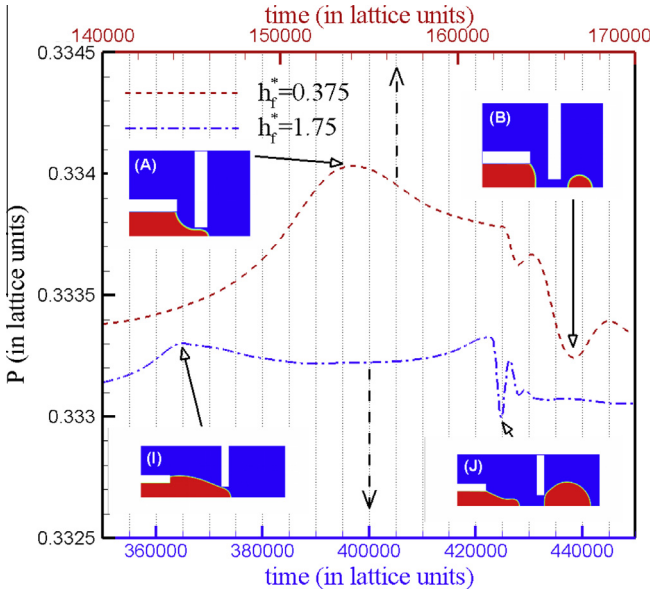

Fig. 11. Pressure variation for two different geometries corresponding to $h_f^* = 0.375$ and 1.75 for $Ca = 0.01$, $l_{or}^* = 0.25$ and $d^* = 0.375$. Inset images show the contours of density at selected time instants shown by the arrows for the upper half domain only. The abscissa for the former is on top (in red) and for the latter is at the bottom (in blue) and are indicated by dotted arrows. (For interpretation of the references to color in this figure legend, the reader is referred to the web version of this article.)

time instant, the dispersed phase droplet is pinched off, as shown in inset (B).

The formation of droplets for $h_f^* = 1.75$ follows a different route. Since the orifice opening is farther away from the dispersed channel, the dispersed phase takes a longer time to be directed into the orifice entrance. This is corroborated with the pressure profile shown in Fig. 11 (blue). Moreover, the dispersed phase occupies a larger space upstream of the orifice. Due to the increased length of the continuous-dispersed phase interface (inset (I)), the squeezing of the emerging bulb takes a longer time. Thus, in this case the droplet formed is larger than the channel widths at the inlet of the liquid steams with a spherical shape, similar to the squeezing regime in T-junction geometry [7,15]).

Thus, the dependence of droplet size on distance of the orifice from the continuous phase channel inlet is dictated by the formation of the dispersed phase bulb. This bulb collects the dispersed phase in itself till the leading edge of the interface reaches the orifice entrance. For smaller h_f^*, the dispersed phase liquid stream takes a shorter time to break up as the bulb that is formed before the orifice is smaller, while the liquid stream takes a longer time to break up because of the formation of a bigger bulb before the orifice for larger h_f^*. Therefore, a larger droplet will be formed when a larger bulb is formed upstream of the orifice.

4. Conclusions

In this work, the role of geometry of a microfluidic flow-focusing device on size and shape of droplets formed in an orifice has been investigated. The lattice Boltzmann method was chosen for conducting the parametric study in the microfluidic flow focusing device. A diffuse interface model for biphasic flow was employed to model the flow in the microfluidic device. The method has the ability to accommodate surface topology changes including interface break-up and coalescence. Another attractive feature of the model is the small magnitude of spurious currents that occur at the interface of the two fluids.

Simulations for various geometries of the flow-focusing microfluidic device were conducted to isolate the effect of parameters on the size of droplets and mechanism of their formation. Specifically, the effect of orifice width, orifice length and distance of the orifice on the mechanism of droplet formation and size of droplets is presented for different Capillary numbers corresponding to $Ca = 0.005$, 0.0075 and 0.01. For this study, the flow rate and viscosity ratios were kept fixed, while the Reynolds number was maintained to be less than unity throughout.

Simulations revealed that droplet formation for all geometries occurred due to pressure build-up in the continuous phase, the interplay between this pressure and interfacial force and squeezing of the interface eventually. The duration of pressure acting against the interfacial tension was dependent on the geometry. Moreover, for the same geometry, droplets size decreases as the Capillary number increases.

On comparison of droplet sizes obtained for different orifice lengths, it was observed that on shortening the orifice length, the size of droplets grew exponentially, while for a long orifice it approached a constant value. For the former, the pressure build-up in the continuous phase was gradual, reaching a maximum when the dispersed phase completely blocked the orifice. For the latter, the dispersed phase penetrated the orifice section and remained confined by the solid walls, hence leading to pinch-off even before the dispersed phase reached to the end of the orifice. These results indicate that orifice lengths longer than a critical length do not have any effect on the throughput from the device.

The study on the dependence of orifice width on droplet size revealed that the size of droplets formed increases non-linearly with increasing width. It was shown that the decrease in confinement of the dispersed liquid due to a larger orifice width plays a crucial role in determining the size of the droplet. Physically, the pressure in the continuous phase stream is not allowed to build up sufficiently for a channel with larger orifice width due to which squeezing of the plug is slow, resulting in the formation of a large spherical droplet.

Finally, varying the distance of the orifice from the inlet disclosed that the droplet size increases as the distance of the orifice from continuous phase channel is increased. Moreover, the effect of Ca on droplet size is only pronounced when the orifice is placed at a distance more than the dispersed phase channel width. For orifices closer to the channel inlets, a rapid rise in pressure leads to the interface being pushed towards the center of the orifice and a relatively smaller droplet is formed. For larger distances, the dispersed phase takes a longer time to be directed into the orifice entrance due to an elongated interface resulting in a larger

spherical droplet being formed, similar to the squeezing regime in a T-junction geometry.

It is anticipated that the trends generated in this study will facilitate tuning of the architecture and act as a driving force for further research in exploring the dynamics of the flow-focusing device.

References

[1] Christopher GF, Anna SL. Microfluidic methods for generating droplet streams. J Phys D: App Phys 2007;40:R319–36.
[2] Stone HA, Stroock AD, Ajdari A. Engineering flows in small devices: microfluidics towards a lab-on-a-chip. Ann Rev Fluid Mech 2004;36:381–411.
[3] Cramer C, Fischer P, Windhab EJ. Drop formation in a co-flowing ambient fluid. Chem Engg Sci 2004;59:3045–58.
[4] Umbanhowar PB, Prasad V, Weitz DA. Monodisperse emulsion generation via drop break off in a coflowing streams. Langmuir 2000;16:347–51.
[5] Garstecki P, Fuerstmann MJ, Stone HA, Whitesides GM. Formation of droplets and bubbles in a microfluidic T-juncton-Scaling and mechanism of break-up. Lab Chip 2006;6:437–46.
[6] Guillot P, Colin A. Stability of parallel flows in a microchannel after a T-junction. Phys Rev E 2005;72:066301.
[7] Gupta A, Kumar R. Effect of geometry on droplet formation in the squeezing regime in a microfluidic T-junction. Microfluidics Nanofluidics 2010;8:799–812.
[8] Gupta A, Kumar R. Flow regime transition at high Capillary numbers in a microfluidic T-junction: viscosity contrast and geometry effect. Phys Fluids 2010;22:122001.
[9] Gupta A, Murshed SMS, Kumar R. Droplet formation and stability of flows in a microfluidic T-junction. App Phys Lett 2009;94:164107.
[10] Thorsen T, Roberts RW, Arnold FH, Quake SR. Dynamic pattern formation in a vesicle-generating microfluidic device. Phys Rev Lett 2001;86:4163–6.
[11] Anna SL, Bontoux N, Stone HA. Formation of dispersions using 'flow-focusing' in microchannels. App Phys Lett 2003;82:364–6.
[12] Dupin MM, Halliday I, Care CM. Simulation of a microfluidic flow-focusing device. Phys Rev E 2006;73:055701(R).
[13] Garstecki P, Fuerstman MJ, Whitesides GM. Nonlinear dynamics of a flow-focusing bubble generator: an inverted dripping faucet. Phys Rev Lett 2005;94:234502.
[14] Jensen MJ, Stone HA, Bruus H. A numerical study of two-phase Stokes flow in an axisymmetric flow-focusing device. Phys Fluids 2006;18:077103.
[15] Romero PA, Abate AR. Flow focusing geometry generates droplets through a plug and squeeze mechanism. Lab Chip 2012;12:5130–2.
[16] Zhou C, Yue P, Feng JJ. Formation of simple and compound drops in microfluidic devices. Phys Fluids 2006;18:092105.
[17] Chen S, Doolen GD. Lattice Boltzmann method for fluid flows. Ann Rev Fluid Mech 1998;30:329–64.
[18] Lishchuk SV, Care CM, Halliday I. Lattice Boltzmann algorithm for surface tension with greatly reduced microcurrents. Phys Rev E 2003;67:036701.
[19] Latva-Kokko M, Rothman DH. Diffusion properties of gradient-based lattice Boltzmann models of immiscible fluids. Phys Rev E 2005;71:056702.
[20] Rowlinson JS, Widom B. Molecular theory of capillarity. New York: Dover Publications; 1982.
[21] Shi Y, Tang GH, Xia HH. Lattice Boltzmann simulation of droplet formation in T-junction and flow focusing devices. Comp Fluids 2014;90:155–63.
[22] Succi S. The lattice Boltzmann equation for fluid dynamics and beyond. New York: Oxford University Press; 2001.